Implementation of stochastic approach for vessel and ridge studies in retinopathy of prematurity screening

S. Prabakar[1,*], K. Porkumaran[1], Parag K. Shah[2] and V. Narendran[2]

[1]Department of Biomedical Engineering, Dr N.G.P. Institute of Technology, Coimbatore 641 048, India
[2]Department of Paediatric Retina and Ocular Oncology, Aravind Eye Hospitals, Coimbatore 641 014, India

The retinopathy of prematurity (ROP) is an ocular pathological disorder of retinal blood vessels in premature infants and low birth weight infants. The medical professional who is taking care of premature infants should know who is at the risk of this disease and its exact severity stage. It is also important to decide when screening must begin and how often these infants need to be examined as disease progression leads to a more severe stage causing blindness. The contrast stretching method has been utilized to enhance the ROP colour image. Then an automatic isotropic undecimated wavelet transform (IUWT) scheme has been proposed to extract the abnormal retinal blood vessel and measure its width and tortuosity. The ridge formation of this pathological disorder has also been extracted by IUWT. The quantitative measurements of mean diameter, standard deviation, tortuosity, length of retinal blood vessel and ridge have been considered and computed to find the exact severity stage of ROP. The proposed methods for ROP stage screening system have been validated through machine vision techniques. This proposed system improves the optimum time utilization for ophthalmologists; ophthalmic technicians can provide exact ROP stage and deliver better accuracy and sensitivity in diagnosis.

Keywords: Isotropic undecimated wavelet transform, retina vessel and ridge, retinopathy of prematurity, tortuosity.

MODERN opthalmology utilizes image processing, investigation and computer vision techniques for exact diagnosis. Retinopathy of prematurity (ROP) is a pathological disorder when abnormal blood vessels develop at the edge of normal retinal blood vessels in premature infants. It is characterized by blood vessel width, tortuosity of the vessels and ridge formation in various zones in the retinal area. The optic disk, macula and fovea are important landmarks for zone selection and cater to the severity level of ROP. A hybrid automated retinal vessel and ridge segmentation method is discussed here. The measurement of features such as tortuosity, width, length of abnormal retinal vessel and ridges has been utilized to screen ROP stages[1]. The immature retinal vascular structures are distressed by the ROP disease in premature infants[2,3]. The high risk pre-threshold stage of ROP can cause blindness in premature infants[4]. ROP at the initial phase does not have any visual defects but can become aggressive with neovascularization. At the extensive progressive stage, the detachment of retina occurs leading to blindness[5]. Infants who weigh less than 1800 g at birth or are born before 32 weeks gestation period are at higher risk of ROP occurrence[6,7]. The exact time to begin screening and how often infants need to be examined has to be decided for the infants at risk. Based on screening, ophthalmologists decide when to treat ROP infants and what long term follow-up is essential to manage other complications of ROP[8,9].

*For correspondence. (e-mail: srisornaprabu@gmail.com)

Classification and severity stages of ROP

Retinal blood vessels develop from the optic disc out towards the periphery. From the flattened retina, the progression of the disease is classified based on location of the disease presence as referred by ICROP (ref. 3). Generally, Zone-I disease is the most precarious and may lead to retinal detachment and further can cause blindness. Also, Zone-II is more severe than Zone-III disease. The Retcam images are analysed by ophthalmologists to diagnose various severity stages of ROP. ROP is a rapidly progressive disease which starts slowly, usually anywhere from the fourth to the tenth week of infant's life and may progress through successive stages, from stages 1 to 5 (refs 10, 11).

The familiar ROP severity stage classification (Figure 1) is described as follows. Stage 1: A-vascular retina is separated from the vascularized retina posteriorly by a thin, white, flat demarcation line. Stage 2: The ridge which is an extended flat line developed in height, width and volume from stage 1 turned out to be pink-white ridge. Stage 3: The posterior aspect of the ridge contains continuous extra-fibrovascular proliferating tissue; immediately posterior to the ridge or extending directly into the vitreous. Stage 4: Partial retinal detachment drags the

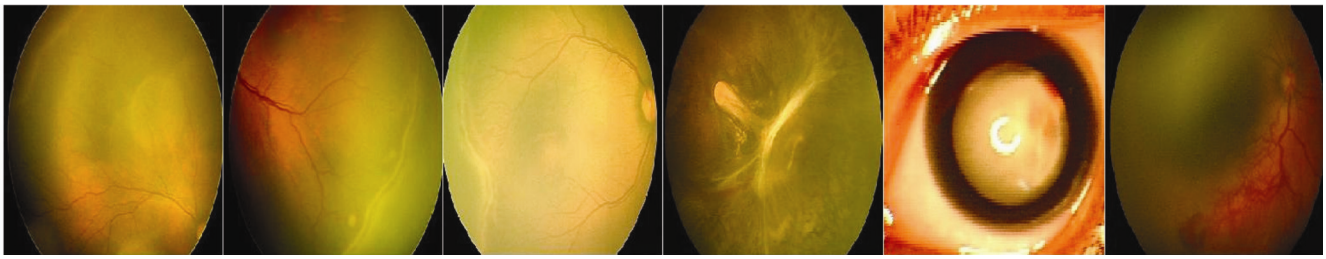

Figure 1. Sequence of ROP images for stages 1–5 and plus disease.

vessels which lead to retinal detachment. Stage 5: Total retinal detachment is observed with ultrasonographic scans.

Plus disease: The presence of dilated posterior veins, tortuous retinal arteries, vitreous haze and pupillary rigidity; it is represented as '+' disease ROP. It denotes a high risk of ROP and the patient must be monitored closely and carefully.

Analysis of retinopathy related work

Ophthalmologic disorders are accurately diagnosed based on automated fundus image analysis in computer-aided diagnosis. The inception and progression of diseases such as diabetic retinopathy (DR), maculopathy, ROP, etc., are diagnosed by changes in retinal vessel morphology. However, detecting blood vessels in retinal fundus images with the presence of bright and dark lesions is a challenge which requires intelligent image processing methodologies.

Healthy and unhealthy retinas have been simultaneously handled by a novel multiconcavity modelling approach which delivered attractive performance on a mixture of healthy and pathological retinas[7]. Sofka and Stewart[12] have proposed a new technique for extracting low-contrast and narrow vessels to eliminate false detections at non-vascular structures.

ROP, hypertension, stroke, diabetes and cardiovascular diseases prelude tortuosity as the most significant symptom. An early detection of retinopathies requires automatic evaluation and quantification of retinal vessel tortuosity. Tudor *et al.*[13] proposed an approach based on principal component analysis (PCA), for evaluation of tortuosity in vessels extracted from digital fundus images. Further, numerical integration method (NIM) and numerical differentiation method (NDM) were implemented for automatic tortuosity evaluation. The K-nearest neighbour classifier produced 87.3% accuracy in the estimated results against ground truth from ophthalmologists.

Bankhead *et al.*[14] proposed an algorithm for efficient detection and measurement of retinal vessels from both low and high resolution fundus images and fluorescein angiograms. The image profiles have been computed perpendicularly across a spline fit of each detected vessel centreline to locate the vessel edges. Carmen and Domenico[15] have proposed self-organizing maps (SOM), K-means clustering and Fuzzy C-means clustering for segmentation of retinal vessels.

Many retinal diseases are characterized by extreme changes in retinal vessels like ROP plus disease. Conor Heneghan *et al.*[9] developed a general technique for segmenting vascular structures in retinal images and characterizing segmented blood vessels. The segmentation technique involved morphological preprocessing and second derivative operator to emphasize the linear and thin vascular structures.

Jomier *et al.*[11] developed geometric information by considering blood vessels as tubes and measured the extracted tortuosity and dilation. Retinal eye diseases like hypertensive retinopathy (HR), DR, glaucoma, etc., are detected by fundus image analysis. Parameters such as segmentation of blood vessels, measurement of tortuosity, diameter measurement, artery vein ratios (AVR) are used to find HR using digital fundus images[16]. Wilson *et al.*[17] proposed a software for measuring tortuosity, width of retinal veins and arteries from digital ROP images. A semiautomatic computer-aided image analysis of the retina (CAIAR) program was developed to detect retinal vasculature and measurement.

In general, the supervised algorithms segment the vessels and ridges with higher computation time. In many cases of retinal images, these efficient supervised algorithms could not be used to enhance the image, because of huge variations in image acquisition. Simple thresholding operation could be used to identify retinal vessels and ridges[11]. On the other hand, unsupervised algorithms have been combined with the automatic optimization of parameters which have been utilized to obtain faster results with new image types[18,19]. The manual detection of tortuosity, vessel and ridge width to screen the severity level of ROP is a time-consuming procedure and the ophthalmologist may get fatigue on scanning and analysing the ROP images[20].

By reviewing all methods, an unsupervised stochastic algorithm has been proposed for ROP screening. This has two stages, the first stage using wavelet schemes deals with detection of blood vessels, measuring tortuosity and vessel width from the ROP RETcam image using third level decomposition. The next stage of fourth level decomposition deals with ridge parameters such as

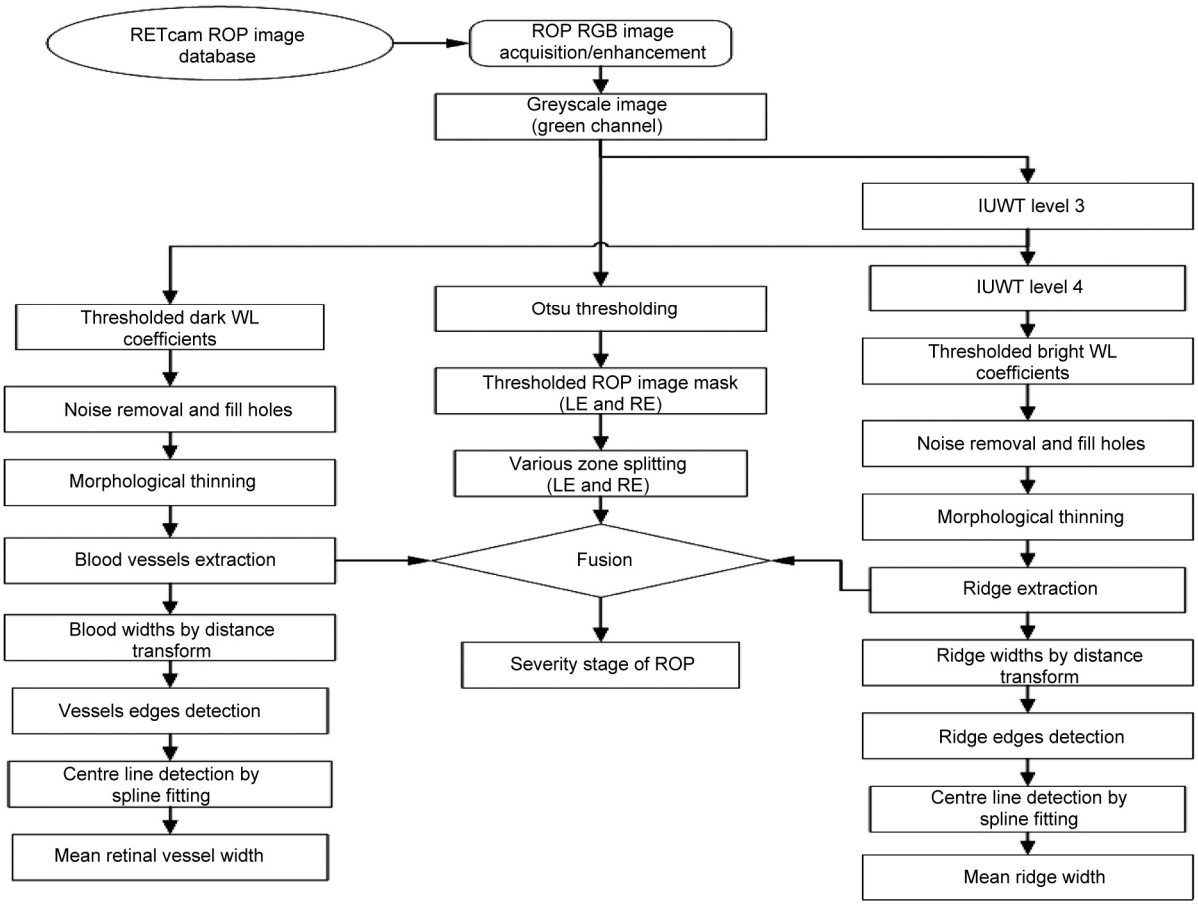

Figure 2. General block diagram of wavelet based ROP screening system.

location, length and width in various zones in the retinal images. Thus, the estimated parameters of vessel and ridge have been utilized to detect the disease severity level of ROP. The implementation of proposed automatic machine vision algorithms using computer simulation tool will reduce manual investigation complications.

Materials and methods

Literature review described many clinical procedures and imaging algorithms to study retinal fundus images. All the proposed methods have their own merits and demerits depending on the application on ROP image analysis. To overcome the disadvantages and ensure efficient quantification of retinal vessels and ridges presented in the ROP images, a new wavelet based methodology has been proposed in this study. This method considers various parameters of retinal vessels and ridges to efficiently screen the severity stages of ROP.

The premature infant retinal images were obtained from the paediatric section of Aravind Eye Hospital (Coimbatore). The digital retinal images have been captured by RetCam-120; MLI Inc., Pleasanton (California) at 130° field of view. A minimum of five retinal images for each right and left eye of the premature infants were collected and considered to accomplish the proposed algorithm. These raw colour images are in .hdr or .bmp format with a size of 640×480 pixels. In all cases, colour images were converted to gray scale by extracting the green channel components, because the green channel revealed the best contrast for vessel detection. Before the gray scale conversion of the colour retinal image, the brightness, colour and contrast of the image were enhanced with mean intensity adjustment and contrast stretching method. This process improved the appearance of retinal blood vessels and ridge formation in ROP images. Further, a minimized mask was created to exclude the unnecessary parts of the image to improve the accuracy level on the boundary detection.

The two-dimensional isotropic undecimated wavelet transform (IUWT) has been proposed for the gray scale ROP images to analyse the blood vessel by third iteration and ridges by fourth iteration (Figure 2). Consecutively, the dark vessel thresholding (16–20%) or bright vessel thresholding (13–17%) has been applied to extract the retinal vessel and ridges respectively. Various numerical parameters such as length, width, tortuosity of the

segmented vessel and ridge have been measured by different mathematical computations. These parameters cater to the appropriate severity level ROP disease. The Otsu thresholding technique has been utilized to develop the retinal mask and define the various zones of the retina. The optic disk and fovea localization has been obtained to define the exact zones in the retina. The fusion of extracted ridge with zones and diameter of the ridge information indicate the proper severity stage of the ROP.

Two-dimensional isotropic undecimated wavelet transform

The multiscale method is an expansion of wavelets in which decimated Bi-orthogonal wavelet transform (DBWT) has been used in many medical image applications. But DBWT has loss of translation invariance property which leads to a large number of artefacts in its results. So, this technique is not mostly preferred for analysis of biological data. An undecimated transform for thresholding which improves the result by more than 2.5 dB in denoising applications has been proposed[21–25]. The undecimated wavelet transform and its reconstruction consist of the standard undecimated wavelet transform and IUWT[26,27]. The undecimated wavelet transform, particularly IUWT and its reconstruction has been described in this section. Then the specially designed filter bank for IUWT decompositions has been utilized to process artefacts in ROP images.

IUWT algorithm is more suited for retinal image analysis, because the objects are more or less isotropic in most cases. The requirements for a good analysis of such data are as follows. Filters must be symmetric

$$\hat{h}[k] = h[k] \text{ and } g[k] = g[k]. \tag{1}$$

In two dimension or higher dimension, h, g, ψ, ϕ must be more or less isotropic.

Consider a real discrete-time filter whose impulse response is $h[n]$, $\hat{h}[n] = h[n], n \in \mathbb{Z}$ is its time reversed version. For wavelet representation and analysis, filters are denoted as h and g and the scaling and wavelet functions are denoted as ϕ and ψ respectively. Filters need not be orthogonal or bi-orthogonal, so that the separability $h[k, l] = h[k]h[l]$ has been considered for fast calculations for huge volume of data set. For wavelet theory at each iteration i, scaling coefficient c has been computed by low pass filtering and wavelet coefficients w_i by subtraction. The related filters h and g are defined by

$$h^{1D}[k] = \frac{[1,4,6,4,1]}{16}, k = -2,...,2, \tag{2}$$

$$h[k, l] = h^{(1D)}[k]\, h^{(1D)}[l], \tag{3}$$

$$g[k, l] = \delta[k, l] - h[k, l], \tag{4}$$

where δ is defined as $\delta[0, 0] = 1$ and $\delta[k, l] = 0$ for all (k, l) different from (0, 0). Also, the filter $h_0 = [1, 4, 6, 4, 1]/16$ is obtained from the cubic B-spline. The mean original signal is conserved by scaling coefficients. But the wavelet coefficients have a zero mean and information has been encoded for different spatial scales present within the signal. This has been applied to a signal c_0, and the subsequent scaling coefficients are calculated by convolution with a filter h^{ui}. h^{ui} is the up-sampled filter obtained by inserting $2^i - 1$ zeros between each pair of adjacent coefficients of h_0.

$$c_i = c_i * h^{ui}. \tag{5}$$

Filtering has to be applied in all directions when the original signal c_0 is multidimensional. The finite impulse response filters (h, $g = \delta - h$) should follow certain even symmetric properties using FIR filters. Based on the structure of g, the wavelet coefficients have been obtained by calculating the difference between two resolutions

$$w_{(i+1)}[k, l] = c_i\,[k, l] - c_{(i+1)}[k, l], \tag{6}$$

where $c_{(i+1)}[k, l] = (\hat{h}(i)\hat{h}(j) * c_i)[k, l]$.

One set of $\{w_i\}$ has been obtained for each scale of i. The addition wavelet scales and smoothed array reconstructs the ROP image.

$$c_0[k, l] = c_J[k, l] + \sum_{i=1}^{I} w_i[k, l]. \tag{7}$$

So the reconstruction of the original signal from all wavelet coefficients and the final set of scaling coefficients required only the addition. After computing n wavelet levels.

$$c_0 = c_n + \sum_{i=1}^{n} w_i. \tag{8}$$

The synthesis filters $\tilde{h} = \delta$ and $\tilde{g} = \delta$ are FIR based on the symmetric filter properties. This wavelet transformation has been adopted for analysis of ROP images which contain isotropic objects. Features such as retinal vessels and ridges have become visible with improved contrast on higher wavelet levels. Especially wavelet level 3 has been adopted for better blood vessel visibility and level 4 to visualize ridges on ROP images. The wavelet levels exhibit the best contrast to be added and thresholding has been applied to lowest valued coefficients to carry out the segmentation of vessels and ridges in ROP images. The

field-of-view (FOV) has been estimated for an ROP image and the thresholds computed from pixels within the FOV.

The wavelet levels and thresholds need not be changed for all fixed sizes of retinal images. But to extract the blood vessel from all ROP images, the wavelet level has to be chosen to third level decomposition and the threshold has to be fixed as 18–23% of lowest coefficients. Similarly, to extract the ridges from ROP images, the wavelet levels and threshold have been chosen to fourth level and 15% respectively, and the inverted binary image has been preferred to obtain the perfect ridge.

Vessel width and ridge width measurement

The vessel width and ridge width measurement strategy consist of two stages of processing, the middle line estimation and edge identification. The morphological thinning algorithm has been proposed to extract the middle line of the vessel and ridge. The exterior pixels on the identified retinal vessels are iteratively eliminated by the thinning algorithm. The vessel centres are obtained by the connected lines of 'on' pixels along the entire length of the vessel[28–31].

The end pixels which have less than 2 neighbours are identified which are described as the branch in the vessels. In the proposed method, many monotonous middle lines have been eliminated as much as possible by removing the short segments which have less than 10 pixels. Further, the pixels which have greater than 2 neighbours are also removed. The unnecessary spur which produced side-effect on thinning process and end-bifurcated vessels has also been eliminated. The vessel widths are coarsely estimated in the inverted binary ridge image using distance transform. The connected pixels represented the middle line and edges of a possible vessel and ridge segment which could be used for further analysis of ROP screening. The smooth middle line could be obtained as shown in Figure 3, using a parametric spline curve based on the centripetal scheme.

The edge points of vessels and ridges are estimated to compute the vessel and ridge widths respectively. At any point, the segmented vessel orientation is estimated from the middle line. The ROP vessel and ridge profiles have resemblance of Gaussian functions which have been defined using gradients. The second derivative of accurate zero crossings identified as sub-pixels at a local maximum or minimum derives the edge of vessels and ridges. Otherwise the widths have been defined as the rising edge and the falling edges. The average vessel or ridge width has been estimated from binary profiles.

The median of the sums of vessel pixels of each profile is estimated to derive the temporary width. Then the average of all the vessel profiles has been calculated to identify the locations of the maximum and minimum gradient to the left and right of the centre respectively. An anisotropic Gaussian filter and connected components are used to reduce noise and the possible edges into distinct trails have been linked. The zero-crossings at each side of the vessel centers have been estimated as edges for all trails. The diameter is simply the Euclidean distance between these edges adopted to estimate the vessel and ridge as represented in Figure 3.

Results and discussion

The ROP severity has various stages from stages 1 to 5, plus disease and aggressive progressive ROP. This research work considered the ROP images up to stage 3 and plus disease to develop the ROP screening system. Obviously stages 4 and 5 are the most severe stages and the baby may not get a clear vision although proper clinical procedures are followed with utmost care. IUWT has been applied for stage 1 to stage 3 ROP images and the ridges were extracted by the fourth level of wavelet decomposition. The threshold has been defined to 15% with bright vessel selection. Almost in all cases the ridges were looking brighter than other locations. If the ridges are compared with retinal vessels in ROP images, they have inverse intensity and resolution property of the images.

The present work considered 52 premature infants who have ROP issues at various stages. Each infant's retinal images (in total 260 ROP images) have been acquired with RetCam at the Aravind Paediatric Ophthalmology

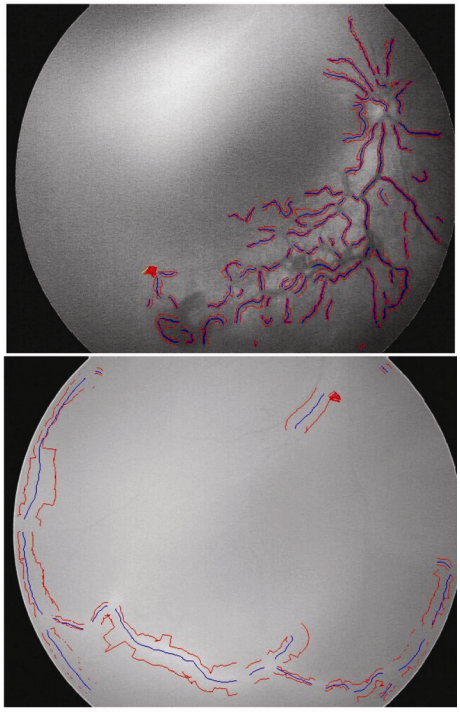

Figure 3. Representation of middle line (blue) and edges (red) of vessels and ridges.

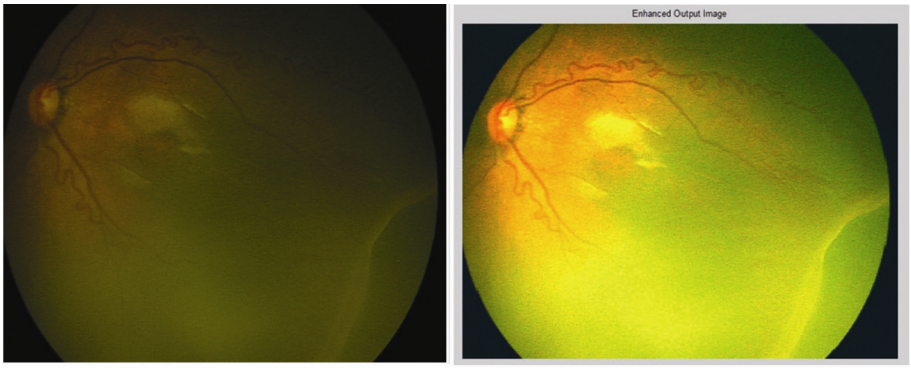

Figure 4. Original RetCam ROP image and contrast enhanced image.

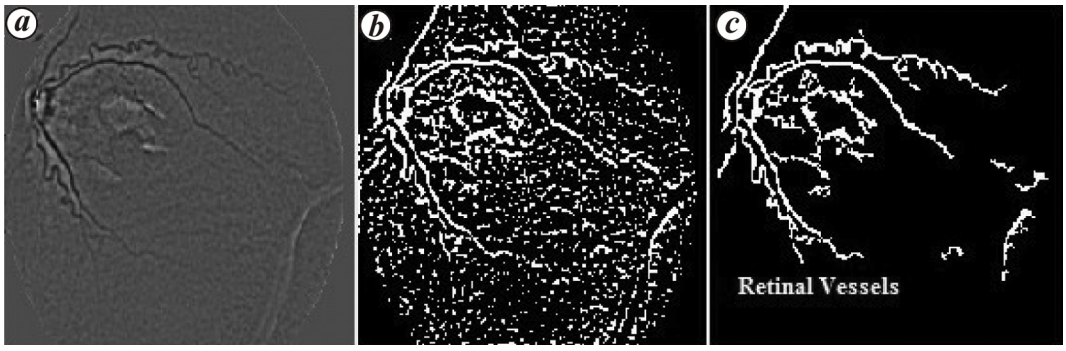

Figure 5. ***a***, IUWT level 3 applied image; ***b***, Thresholded image; ***c***, Segmented retinal vessels.

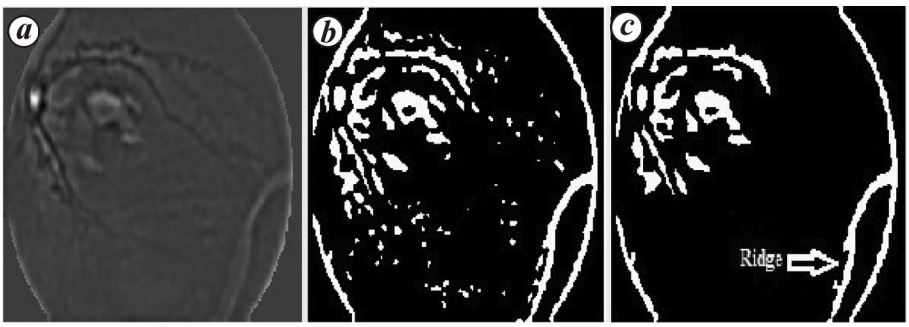

Figure 6. ***a***, IUWT level 4 applied image; ***b***, Bright thresholded image; ***c***, Segmented ridge structure.

Center (Coimbatore) using regular ROP screening procedures. The ophthalmologist's proficiency level plays a vital role in ROP severity screening. Based on the clinical features of ROP images, IUWT has been adopted for left eye and right eye images to extract vessels and ridges and measure the widths. ROP images obtained from RetCam are in .hdr or .bmp file format with the size of 640 × 480. These unprocessed images have been preprocessed to enhance the contrast of retinal vessels and ridges (Figure 4). These images have been considered as the input for the proposed IUWT based system.

This work involved two main steps: the first step included the much faster unsupervised vessel and ridge segmentation by thresholded wavelet coefficients, which would achieve better accuracy and less computation time when compared with other existing techniques. The second step included a graph-based algorithm to extract middle lines and locate the vessel edges and ridge edges from ROP images. Spline fitting has been used to determine the vessel or ridge orientation. The detection of zero crossings of second derivative at right angles to the vessel or ridge has been utilized to extract the middle line and edges. The various IUWT iteration levels have been implemented for input ROP images. It was observed that the level 3 iteration delivered satisfactory output on retinal vessels. Then the dark thresholding was selected to 20% to extract dark blood vessels. The output has more unwanted noise, so that simple morphological functions

Table 1. Various properties of stage 1 ridge measurement

Case	Eye	Number of widths	Mean width (mm)	Standard deviation	Minimum ridge width (mm)	Maximum ridge width (mm)	Ridge length (mm)	Tortuosity
1	LE	150	1.26	0.35	0.57	1.85	40.25	1.04
	RE	224	1.87	0.64	0.59	3.19	61.14	1.49
2	LE	36	0.93	0.24	0.56	1.39	9.83	1.04
	RE	56	2.48	0.27	1.97	3.03	14.62	1.04
3	LE	75	1.43	0.38	0.67	2.24	22.04	1.77
	RE	39	0.99	0.39	0.46	1.58	11.40	1.00
4	LE	27	2.59	0.45	2.14	3.56	7.64	1.01
	RE	154	3.08	0.82	1.61	4.98	41.39	1.12
5	LE	32	1.48	0.28	0.83	2.06	14.09	1.04
	RE	32	2.70	0.39	2.30	3.41	8.15	1.03
6	LE	66	1.63	0.57	1.00	2.75	17.21	1.04
	RE	40	2.89	0.46	2.52	4.02	10.48	1.06
7	LE	42	1.32	0.40	0.56	1.90	12.13	1.05
	RE	47	2.26	0.53	0.93	3.12	11.88	1.21
8	LE	31	2.02	0.56	0.92	2.69	10.01	1.02
	RE	27	1.49	0.14	1.22	1.66	7.51	1.01
9	LE	171	1.75	0.57	0.39	3.18	52.94	1.25
	RE	300	2.11	0.63	0.70	3.39	86.89	1.02

Table 2. Various properties of stage 2 ridge measurement

Case	Eye	Number of widths	Mean width (mm)	Standard deviation	Minimum ridge width (mm)	Maximum ridge width (mm)	Ridge length (mm)	Tortuosity
1	LE	356	1.56	0.44	0.58	2.46	98.68	1.36
	RE	466	1.98	0.65	0.47	3.64	129.12	1.19
2	LE	246	1.93	0.62	0.63	3.57	66.79	1.07
	RE	336	2.72	0.82	0.71	4.43	90.26	1.04
3	LE	137	1.27	0.33	0.64	1.93	37.85	1.02
	RE	317	2.14	0.75	0.95	4.29	86.25	1.06
4	LE	156	5.52	1.02	2.97	7.14	42.16	1.10
	RE	165	5.43	1.42	3.48	8.05	25.89	1.05
5	LE	33	3.04	0.21	2.81	3.43	44.83	1.15
	RE	57	2.82	0.58	1.96	3.95	9.21	1.11
6	LE	250	1.80	0.60	0.50	3.38	19.81	1.03
	RE	112	2.03	0.72	0.72	3.15	66.95	1.06
7	LE	303	2.62	0.77	0.43	4.02	29.28	1.02
	RE	112	2.63	1.05	0.60	4.71	80.94	1.05
8	LE	145	1.68	0.49	0.74	2.71	29.93	1.86
	RE	357	1.39	0.55	0.18	2.67	39.28	1.15
9	LE	134	3.31	1.11	1.40	5.38	110.64	1.09
	RE	259	3.80	1.34	1.49	6.28	37.43	1.05
10	LE	198	1.88	0.84	0.41	4.00	70.29	1.18
	RE	95	1.87	0.41	0.75	2.66	54.36	1.11

such as erosion, dilation, connectivity and blob filling techniques were utilized to obtain the optimum retinal vessel structures as shown in Figure 5. The tortuosity level of the retinal vessels was estimated for the required vessel portions by a manual selection process, i.e. relative length variation method.

IUWT iteration was extended from third level to fourth level to extract the available ridges in ROP images. In this process, instead of dark thresholding, bright thresholding was chosen to 15% to extract the ridges. Similar morphological operators have then been proposed to extract ridges and the ridge portions alone have been

Table 3. Various properties of stage 3 ridge measurement

Case	Eye	Number of widths	Mean width (mm)	Standard deviation	Minimum ridge width (mm)	Maximum ridge width (mm)	Ridge length (mm)	Tortuosity
1	LE	139	5.51	2.04	2.58	9.92	156.32	1.32
	RE	69	5.39	0.73	3.74	6.53	18.45	1.05
2	LE	219	6.50	2.01	3.10	11.28	316.01	1.34
	RE	338	1.24	0.39	0.61	2.40	91.46	1.48
3	LE	118	7.47	0.78	6.05	9.04	32.83	1.05
	RE	254	6.74	1.54	3.03	8.91	68.16	1.05
4	LE	184	3.26	0.64	2.00	4.68	48.10	1.08
	RE	471	4.60	1.26	1.44	6.39	133.75	2.95
5	LE	192	3.34	1.30	1.44	5.97	52.08	1.23
	RE	192	3.13	0.72	1.64	4.76	57.62	1.04
6	LE	168	2.65	1.06	0.70	4.55	48.99	1.02
	RE	134	2.34	0.53	1.23	3.70	35.53	1.10
7	LE	416	2.57	1.19	0.82	6.34	111.29	1.10
	RE	38	5.71	0.21	5.21	5.97	9.46	1.00
8	LE	390	4.14	1.30	1.34	7.21	104.56	1.04
	RE	178	3.92	0.92	1.34	5.75	48.06	1.05
9	LE	148	4.81	1.54	2.76	7.70	39.95	1.21
	RE	148	4.27	0.94	2.73	6.47	41.28	1.05

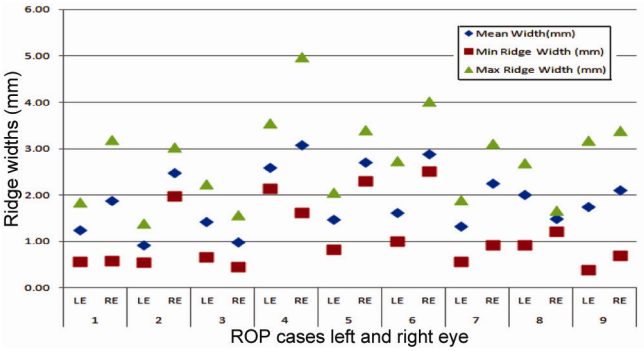

Figure 7. Stage 1 ridge parameters measurement (mean, minimum and maximum width) for different cases left and right eye.

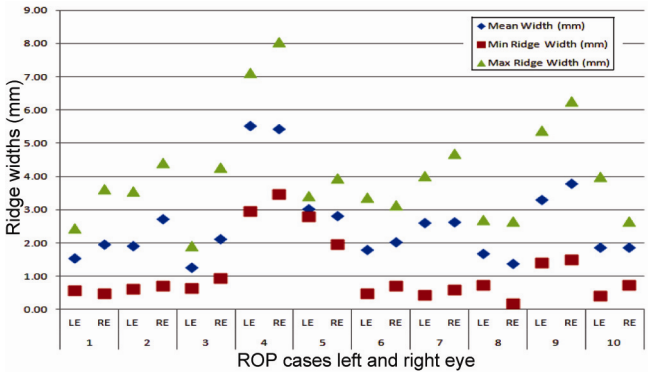

Figure 8. Stage 2 ridge parameters measurement (mean, minimum and maximum width) for different cases left and right eye.

extracted as shown in Figure 6. In this work, one pixel (approximately equivalent to 0.27 mm) has been considered to extract the ridge length from the segmented ridge structure. The properties of a ridge such as maximum and minimum width, mean width, standard deviation and tortuosity levels were then computed to screen the severity stage of ROP. For each and every stage various ridge values have been tabulated as shown in Tables 1–3. The various parameters such as number of widths, mean width, standard deviation, minimum width, maximum width, ridge length, and tortuosity of stages 1, 2 and 3 for the left and right eye of various infants are measured and tabulated. These values played a major role in the ROP severity stage screening.

Figures 7–9 illustrate the various properties of ridges such as mean width, minimum and maximum ridge width versus various individuals suffered with stages 1, 2 and 3 level of ROP diseases. These estimated parameters using proposed algorithm are extremely useful to predict the severity stage of ROP diseases. The ridge width plays a crucial role in severity diagnosis, the developed small demarcation line extends to pink-white ridges and develops to retinal fibrovascular proliferation. The ridge width is smaller in stage 1 severity and increases gradually in stages 2 and 3, when the ROP disease is not properly treated. Stage 3 parameters were measured using the proposed method which has highest span of widths starting from 2.34 to 11.28 mm. The other two stages 1 and 2 had the maximum ridge width of 4.98 and 8.05 mm respectively. The mean ridge width measurements have also specified that stage 3 has more predominant value which is 30–50% higher than the other two stages. Surprisingly, the minimum ridge width measurement indicated that stage 2 has the lowest value, i.e. 0.18 mm when

compared with stage 1 minimum width value i.e. 0.3946 mm. Such deviations may occur in very few cases due to the huge variation in Retcam images. Hence the exact severity stage identification of ROP diseases requires ridge location or zone classification along with the ridge width estimation.

The ridge lengths of various stages with respect to various cases are illustrated in Figure 10. Extensive ridge length was observed in stage 3 cases when compared with other severity stages. This prolonged length may lead to retinal detachment through neovascular generation.

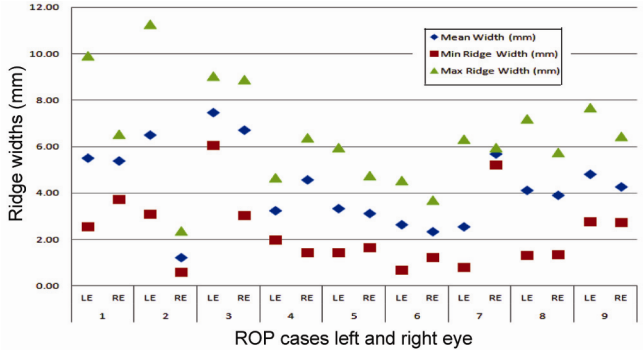

Figure 9. Stage 3 ridge parameters measurement (mean, minimum and maximum width) for different cases left and right eye.

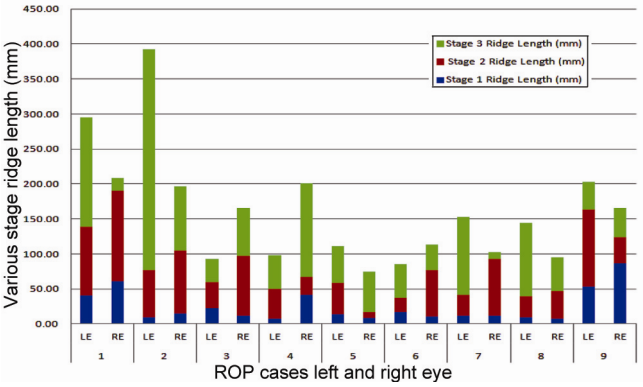

Figure 10. Various stages ridge length measurement for different cases left and right eye.

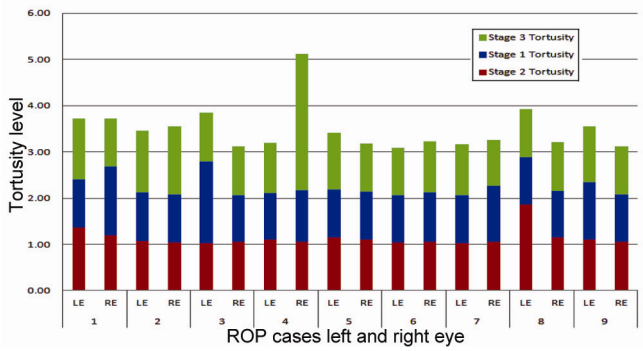

Figure 11. Various stages ridge tortuosity level measurement for different cases left and right eye.

Similarly, Figure 11 symbolized the tortuosity level at various stages against different ROP cases. The increased tortuosity level was observed in stage 3, but the vessel and ridge tortuosity observed in various stages provide the evidence for progressive ROP and ROP plus disease. The proposed ROP screening system considered these ridge and retinal vessel parameters to categorize the exact severity stage of ROP disease.

Conclusion

A stochastic approach has been proposed to detect and measure the properties of blood vessels. Ridges in various stages of ROP images have been described in this paper. This developed algorithm has been implemented for various stages of ROP images. This method could deliver high level of accuracy, low measurement error and short computation time for both low and high resolution images. The outcomes of the IUWT implementation on ROP images delivered the properties of retinal vessels and ridges, which are more suitable than the existing techniques to predict the severity stages of ROP. The various parameter measurement of retinal vessels and ridges for various stages of ROP images have been quantified and further screening done. The measured parameters are more significant for severity estimation; stage 3 has predominant parameters when compared with other stages such as stages 1 and 2. Implementation of this system showed that the ROP screening system could easily identify stage 3 cases and the system felt fuzziness at stages 1 and 2 due to the overlapping values of parameters. The ROP severity stage quantification and screening system produced 93% accurate result on stage 3 and 85% accuracy in stages 1 and 2. The effectiveness of the proposed method has been demonstrated through experimentation using various ROP diseased cases. The outputs from the developed system have been validated with the results of expert ophthalmologists.

The best ROP classification could be achieved by the implementation of efficient soft computing based classifier using retinal vessel and ridge parameters. The thresholding based retinal image mask can be created to classify the various zones in the retina. The fusion of the retinal vessels and ridges with retinal zone mask images could deliver the proper severity stage of ROP. The work could be extended with these techniques and could achieve better results in future. The Graphical User Interface based menu options will also provide user friendly environment for non-ophthalmologists so that the time consumption can be considerably reduced, i.e. instead of analysing all RetCam images, diagnosis with emphasis on the infants who have suffered with severe stage ROP can be provided.

1. Parag K. S., *et al.*, Retinopathy of prematurity – the new challenge. *Retina*, 2011, **17**, 23–27.

2. Wittchow, K., Shared liability for ROP screening. *OMIC J. P.3*, 2003; http://www.omic.com/new/digest/ DigestFall03.pdf
3. Bashour, M., Menassa, J. and Gerontis, C. C., Retinopathy of prematurity. November 2008 (online); http://www.emedicine.medscape.com/article/1225022
4. Early treatment of retinopathy of prematurity cooperative group, revised indications for the treatment of retinopathy of prematurity. *Arch. Ophthalmol.*, 2003, **121**, 1684–1696.
5. International Committee for the Classification of Retinopathy of Prematurity, The International Classification of Retinopathy of Prematurity Revisited. *Arch Ophthalmol.*, 2005, **123**, 991–999.
6. Quellec, G. *et al.*, Optimal wavelet transform for the detection of microaneurysms in retina photographs. *IEEE Trans. Med. Imag.*, 2008, **27**(9), 1230–1241.
7. Lam, B. S. Y. and Yan, H., A novel vessel segmentation algorithm for pathological retina images based on the divergence of vector fields. *IEEE Trans. Med. Imaging.*, 2008, **27**(2), 237–246.
8. Shankar, P. M., Speckle reduction in ultrasound B scans using weighted averaging in spatial compounding. *IEEE Trans. Ultrasonics, Ferroelectrics Frequency Control*, 1986, **33**(6), 754–758.
9. Heneghan, C. *et al.*, Characteriztion of changes in blood vessel width and tortuosity in retinopathy of prematurity using image analysis. *Med. Image Anal.*, 2002, **6**, 407–429.
10. Prabakar, S. *et al.*, Optimized imaging techniques to detect and screen the stages of retinopathy of prematurity. *Human-Centric Machine Vision* (ed. Fabiio, S.), Intech, 2012, pp. 59–80; doi:10.5772/26609.
11. Jomier, J., Wallace, D. K. and Aylward, S. R., Quantification of retinopathy of prematurity via vessel segmentation. Medical Image Computing and Computer Assisted Intervention – MICCAI 2003, Springer Lecture Notes in Computer Science, 2003, vol. 2879, pp. 620–626.
12. Sofka, M. and Stewart, C. V., Retinal vessel extraction using multiscale matched filters, confidence and edge measures. Technical report, Department of Computer Science, Rensselaer Polytechnic Institute, Troy, New York, 2005, pp. 5–20.
13. Tudor, R. *et al.*, A novel approach for quantification of retinal vessel tortuosity based on principal component analysis. In 8th International Conference Electrical Engineering, Electronics, Computer, Telecommunications and Information Technology (ECIT-CON), Thailand, 2011, vol. 1023 (1026), pp. 17–19.
14. Bankhead, P. *et al.*, Fast retinal vessel detection and measurement using wavelets and edge location refinement. *PLOS ONE*, 2012, **7**(3), 1–12; doi:10.1371/ journal.pone.0032435.
15. Carmen, L. A. and Domenico, T., Automatic unsupervised segmentation of retinal vessels using self-organizing maps and *K*-means clustering (eds Rizzo, R. and Lisboa, P. J. G.), Springer Verlag, LNBI 6685, 2011, pp. 263–274.
16. Vermeer, K. A. *et al.*, A model based method for retinal blood vessel detection. *Comput. Biol. Med.*, 2004, **34**(3), 209–219.
17. Wilson, C. M., *et al.*, Computerized analysis of retinal vessel width and tortuosity in premature infants. Investigative opthalmology and visual science, London, 2008, **49**, 3577–3585; doi:10.1167/iovs.07-1353.
18. Robert, K. *et al.*, Fully automatic algorithm for the analysis of vessels in the angiographic image of the eye fundus. *Biomed. Eng.*, 2012, 11–35 (online); doi:10.1186/1475-925X-11-35.
19. Lassada, S. *et al.*, Automated vessels detection on infant retinal images. In Proceedings of the International Conference on Control, Automation and Systems, 2004, pp. 321–325.
20. Fraz, M. M. *et al.*, Blood vessel segmentation methodologies in retinal images – a survey. *Comput. Meth. Prog. Biomed.*, 2012, 407–433.
21. Starck, J. L., Murtagh, F. and Bijaoui, A., Image processing and data analysis: The Multiscale Approach, Cambridge University Press, 1998.
22. Starck, J. L. and Murtagh, F., *Astronomical Image and Data Analysis*, Springer-Verlag, 2002.
23. Starck, J. L. and Murtagh, F., Astronomical image and signal processing. *IEEE Signal Proc. Mag.*, 2001, **18**, 30–40.
24. Starck, J. L., Fadili, J. and Murtagh, F., The undecimated wavelet decomposition and its reconstruction. *IEEE Trans. Signal Proc.*, 2007, **16**, 297–309.
25. Cohen, A., *Numerical Analysis of Wavelet Methods*, Elsevier, 2003.
26. Antoine, J. P. and Murenzi, R., Two dimensional wavelet analysis in image processing. *Phys. Mag.*, 1994, **16**, 105–134.
27. Dutilleux, P., An implementation of the 'algorithme 'a trous' to compute the wavelet transform in wavelets. In *Time–Frequency Methods and Phase-Space* (eds Combes, J. M. *et al.*), Springer, New York, 1989.
28. Lam, L., Lee, S. W. and Suen, C. Y., Thinning methodologies – a comprehensive survey. *IEEE Trans. Patt. Anal. Mach. Int.*, 1992, **14**, 869–885.
29. Olivo-Marin, J. C., Extraction of spots in biological images using multiscale products. *Pattern Recog.*, 2002, **35**, 1989–1996.
30. Lee, E. T. Y., Choosing nodes in parametric curve interpolation. *Comp. Aid. Des.*, 1989, **21**, 363–370.
31. William, E. H. *et al.*, Measurement and classification of retinal vascular tortuosity. *Int. J. Med. Inf.*, 1999, **53**, 239–252.

ACKNOWLEDGEMENTS. We thank Dr N.G.P Institute of Technology and Aravind Eye Care System, Coimbatore, India for providing necessary facilities to carry out this work. The suggestions and comments of anonymous reviewers, which have greatly helped to improve the quality of our paper, are also acknowledged.

Received 15 October 2013; revised accepted 22 January 2016

doi: 10.18520/cs/v112/i03/517-526